A Modified Flux Regulation Method to Minimize Switching Frequency and Improve DTC-Hysteresis-Based Induction Machines in Low-Speed Regions

Ibrahim Mohd Alsofyani, *Member, IEEE*, Keon Young Kim, *Student Member, IEEE*, Sze Sing Lee, *Senior Member, IEEE,* Kyo-Beum Lee, *Senior Member, IEEE*

***Abstract*— Direct torque control (DTC) suffers from flux droop owing to the long zero-voltage vectors at low motor speeds. Previous studies were able to attain flux regulation by imposing the continuous switching of forward and reverse active voltage vectors by causing torque overshoots in the torque hysteresis bands (THBs). This led to an excessive increase in the switching frequency and larger torque and current ripples, thus reducing the drive efficiency. In this paper, a modified flux regulation method is proposed for the classical DTC using a single THB when flux droop occurs in a low-rotor-speed range. The proposed method can protect the DTC from flux droops at low speeds by reducing the duration of zero-voltage vectors and minimizing the number of reverse-voltage vectors. In addition, the proposed strategy is efficient in reducing torque and current ripples while operating at low motor speeds. Furthermore, a significant reduction in the switching frequency is obtained. The effectiveness of the proposed strategy is confirmed by simulation and experimental results.**

***Index Terms*— Direct torque control, flux regulation, induction motor, low speed.**

I. Introduction

DIRECT torque control (DTC) of induction machines (IMs) has become a powerful and popular control scheme since it was introduced by Takahashi and Noguchi [1] and Depenbrock [2] in the 1980s. DTC has become a leading technology in motor drives and therefore was adopted and marketed by ABB in 1995 [3]. Owing to its merits of straightforward implementation, quick dynamic response, and robustness against motor parameters, the DTC has received significant attention in the research community. Nevertheless, the classical DTC also has some drawbacks, and torque ripples and flux droop at low speeds are the two most notable problems.

In the literature, many DTC variations have been proposed to solve the problems of torque ripples and to maintain a fixed switching frequency. A common method is to integrate space vector modulation (SVM) in the DTC, denoted as DTC–SVM. As opposed to the classical DTC, which has a limited number of voltage vectors, SVM can produce random voltage vectors and regulate the torque and flux with a constant switching frequency. Nevertheless, obtaining the reference voltage vector for DTC–SVM is a crucial issue. Various methods have been introduced in this regard such as deadbeat control [3], sliding mode controller [4], and proportional-integral (PI) controller [5]. Although lower torque ripple and constant switching frequency are obtained using DTC–SVM, it requires a high computational burden, knowledge of motor parameters, and rotary coordinate transformation, resulting in more system complexity. This negates the simplicity and robustness of the conventional DTC.

Another DTC variation is based on model predictive control, which has received increasing attention in research communities [7–12]. Different from the conventional DTC, the selection of voltage vectors is attained based on a predefined cost function. There exist several types of predictive control methods, which differ in the principle of voltage vector selection, predictive horizon, and number of applied vectors. Regardless of the intuitive nature and outstanding performance of predictive control, it requires heavy computation and depends intensely on the accuracy of the motor model and parameters [10].

However, it is desired to obtain enhanced performance while preserving the robustness of the classical DTC. To date, there have been various techniques to improve the original DTC with some modifications either in the hardware and control configuration or in the lookup table. In [13]-[14], ABB has used special inverter named ACS600 and included special functions such as flux optimization and flux braking in their commercialized DTC drive. This allows further performance improvement at different speeds, including low speed regions.

Manuscript received May 16, 2018; revised October 11, December 5, 2018; accepted January 26, 2019. This research was supported by a grant (No.20172020108970) from the Korea Institute of Energy Technology Evaluation and Planning (KETEP) that was funded by the Ministry of Trade, Industry and Energy (MOTIE) and the Korea Institute of Energy Technology Evaluation and Planning (KETEP) grant funded by the Korea government (MOTIE) (No.20182410105160, Demonstration and Development of ESS Solution Connected with Renewable Energy against with the weather condition of Middle East Region).

I. M. Alsofyani and K.-B. Lee are with the Department of Electrical and Computer Engineering, Ajou University, Suwon, 16499, Korea (e-mail: alsofyani@ajou.ac.kr; kyl@ajou.ac.kr).

K. Y. Kim is with the Advanced Drive Technology, Anyang, South Korea. (e-mail: maake1026@ajou.ac.kr).

S. S. Lee is with the Department of Electronics and Computer Science, University of Southampton Malaysia, Johor Bahru 79200, Malaysia, and also with the Power Electronics Laboratory, Ajou University, Suwon 16499, South Korea (e-mail: szesinglee@gmail.com).

This article has been accepted for publication in a future issue of this journal, but has not been fully edited. Content may change prior to final publication. Citation information: DOI 10.1109/JESTPE.2019.2897064, IEEE Journal of Emerging and Selected Topics in Power Electronics

Moreover, multilevel inverter-based DTC with larger switching tables has been introduced in the literature [14–22]. This DTC method shows improved performance but causes higher system complexity and intensive computation. The injection of high-frequency triangular signals into the torque errors was proposed by [23],[24], which is known by dithering method. However, this results in an unpredictable switching frequency under different operating conditions.

Over the last few years, flux regulation of the classical DTC at low motor speeds has attracted increasing attention. Flux magnitude droop occurs when the flux magnitude fails to be regulated at low speed [24], thus degrading other motor variables such as torque, speed, and current. Several variations to the original structure [16-17],[25–28] were introduced to solve this problem in the hysteresis-based DTC. For example, the authors in [17] have focused on modifying the predefined lookup table of DTC by adding more voltage vectors to improve sector transitions where the voltage radial component is zero. However, this has led to an increase in the size of the lookup table, and the DTC has become computationally exhaustive. In [25], this problem has been solved by replacing the torque hysteresis controller with a constant switching torque controller (CSTC). According to the analysis in [25], flux droops occur because of the long duration of negative torque slope used to reduce the torque. Consequently, the periods of zero-voltage vectors become longer. However, the approach in [25] requires a systematic design for the proportional integral (PI) controller of CSTC. Recently, a very simple but effective method was proposed in [27],[28] that simultaneously altered the upper and lower torque hysteresis bands in certain low-speed range. Nevertheless, the reduction of both hysteresis bands results in continuous active vector switching with no selection of zero-voltage vectors to achieve flux regulation. This also resulted in high and unnecessary switching frequencies and increased torque and current ripples, thus reducing the efficiency of the system.

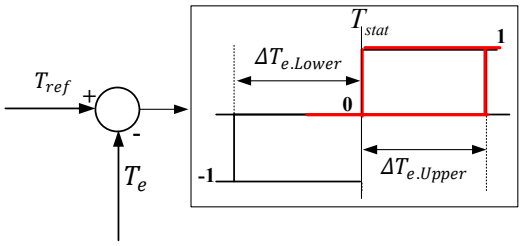

Fig. 1. Structure of the three-level hysteresis comparator.

In this paper, a single-THB control method based on DTC of IMs is proposed to enhance the flux regulation at low-speed operations and to reduce the switching frequency. Unlike previous methods, the proposed scheme focuses on decreasing the negative torque slope to reduce the zero-voltage vectors by the control of a single hysteresis torque band. As such, this method doesn't require the overshoot of torque as in [28]. Hence, the selections of reverse-voltage vectors are minimized and, therefore, the switching frequency is reduced. Moreover, the torque and current ripples are decreased. Simultaneously, the simple configuration of the original hysteresis-based DTC is preserved.

II. PRINCIPLES OF DTC OF INDUCTION MACHINE

A. Model of Induction Machine and variable estimation

The dynamic modeling of an IM can be described through space vector equations in a stationary reference frame where complex space phasors are expressed with vector signs as follows

$$\vec{v}_s = R_s.\vec{\imath}_s + \frac{d\vec{\psi}_s}{dt} \quad (1)$$

$$0 = R_r.\vec{\imath}_r - j\omega_r.\vec{\psi}_r + \frac{d\vec{\psi}_r}{dt} \quad (2)$$

$$\vec{\psi}_s = L_s.\vec{\imath}_s + L_m.\vec{\imath}_r \quad (3)$$

$$\vec{\psi}_r = L_r.\vec{\imath}_r + L_m.\vec{\imath}_s \quad (4)$$

$$T_e = \frac{3}{2}p\frac{L_m}{\sigma L_s L_r}\left|\vec{\psi}_s\right|\left|\vec{\psi}_r\right|sin\delta_{sr} \quad (5)$$

where $\vec{v}_s$ $(=[v_{sd}\ v_{sq}]^T)$ is the stator voltage vectors, which is obtained based on the selection of the switching states (S_a, S_b, and S_c) attained from the switching table [27]. $\vec{\imath}_s$ $(=[i_{sd}\ i_{sq}]^T)$ and $\vec{\imath}_r$ $(=[i_{rd}\ i_{rq}]^T)$ are the stator and rotor currents, and $\vec{\psi}_s$ $(=[\psi_{sd}\ \psi_{sq}]^T)$ and $\vec{\psi}_r$ $(=[\psi_{rd}\ \psi_{rq}]^T)$ are the stator and rotor flux vectors, respectively. ω_r is the rotor motor speed in rad/s. R_s and R_r are the stator resistance and rotor resistance, respectively. L_s, L_r, and L_m are the stator self-inductance, rotor self-inductance, and mutual inductance, respectively. p is the number of pole pairs. δ_{sr} is the load angle between the stator and rotor flux vectors. $\sigma = 1 - L_m^2/L_sL_r$.

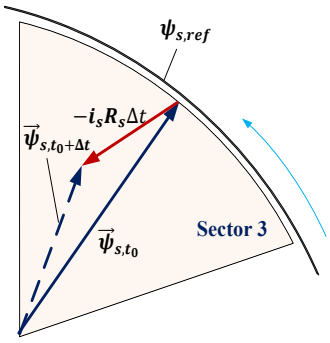

Fig. 2. Effect of voltage drop on the stator flux at low speed.

TABLE I
Voltage Vectors Selection

Flux Demand (ψ_{stat})	Torque Demand (T_{stat})	Voltage Selection
1	1	
	-1	
	0	Zero voltage vectors
0	1	
	-1	
	0	Zero voltage vectors

This article has been accepted for publication in a future issue of this journal, but has not been fully edited. Content may change prior to final publication. Citation information: DOI 10.1109/JESTPE.2019.2897064, IEEE Journal of Emerging and Selected Topics in Power Electronics

In this paper, the conventional current model is employed for the stator flux and torque estimations.

B. DTC at Low Speed

This DTC for a two-level voltage source inverter (2L-VSI) scheme offers a straightforward control configuration. Two hysteresis comparators are employed to separately control the torque and flux. The output from each comparator is sent to a switching table as shown in Table I [1], to determine the appropriate voltage vectors to control both the torque and flux. Fig. 1 shows the structure of a three-level torque hysteresis comparator, which contains an upper hysteresis band ($\Delta T_{e.Upper}$) and a lower hysteresis band ($\Delta T_{e.Lower}$). It is worth mentioning that in most designs of previous DTC schemes, the widths of $\Delta T_{e.Upper}$ and $\Delta T_{e.Lower}$ are equal. The output of the torque comparator or torque error status (T_{stat}) has three states: 1 for forward active-voltage vector, -1 for reverse active-voltage vector, and 0 for a zero-voltage vector.

With a nominal setting of $\Delta T_{e.Upper}$ and $\Delta T_{e.Lower}$ that is usually between 10–15% of the rated torque, the DTC drive works effectively at medium and high speeds. It is well known that a 2L-VSI produces eight voltage vectors $\vec{v}_s = \{\vec{v}_{s,0}, \vec{v}_{s,1} \cdots \vec{v}_{s,7}\}$. Two switching combinations ($\vec{v}_{s,0}$ and $\vec{v}_{s,7}$) determine the zero-voltage vectors, and the remaining combinations generate six active-voltage vectors. Generally, the proper voltage vector is selected in order to preserve the torque and the stator flux within the bounds of two hysteresis bands.

It is possible to obtain the change in the stator flux by rearranging (1) as follows:

$$\frac{d\vec{\psi}_s}{dt} = \vec{v}_s - \vec{\imath}_s R_s \tag{6}$$

$$\Delta\vec{\psi}_{s.Active} \simeq \vec{v}_s \cdot \Delta t \tag{7}$$

Where $\Delta\vec{\psi}_{s.Active}$ is the stator flux variation based on the active voltage vectors. By taking into account the ohmic drop, the flux variation when selecting the zero or null voltage vectors yields

$$\Delta\vec{\psi}_{s.Null} = -\vec{\imath}_s R_s \cdot \Delta t \tag{8}$$

Where $\Delta\vec{\psi}_{s.Null}$ indicates that the change of stator flux is attained when null voltage vectors are chosen. Nevertheless, when the speed decreases to a certain low level, the selection of the null-voltage vectors becomes dominant and significantly reduces the space vector magnitude of the stator flux. An example for the effect of voltage drop on the flux drooping at low speed is illustrated in Fig. 2 when the stator flux vector $\vec{\psi}_{s,t_0}$ moves into $\vec{\psi}_{s,t_0+\Delta t}$ in the anti-clockwise direction in Sector 3. The indices, t_0 and $t_0 + \Delta t$ denote the initial and second time instants, respectively. It can be noted that the stator flux magnitude at $t_0 + \Delta t$ is decreased strongly below the stator reference flux ($\psi_{s.ref}$) owing to the voltage drop across the stator resistance.

The nominal setting of THB used in the torque-hysteresis comparator contributes to the degradation of flux in very-low-speed regions because electric torque slopes have a much greater influence on the stator flux magnitude [23], which are given by

$$T_e^+ = -T_e\left(\frac{1}{\sigma\tau_s} + \frac{1}{\sigma\tau_r}\right) + \frac{3}{2}\frac{p}{2}\frac{L_m}{\sigma L_s L_r} \cdot Im\left(\left(\vec{v}_s \cdot \vec{\psi}_r\right) - j\omega_r\left(\vec{\psi}_s \cdot \vec{\psi}_r\right)\right) \tag{9}$$

$$T_e^- = -T_e\left(\frac{1}{\sigma\tau_s} + \frac{1}{\sigma\tau_r}\right) - \frac{3}{2}\frac{p}{2}\frac{L_m}{\sigma L_s L_r} \cdot Im\left(j\omega_r\left(\vec{\psi}_s \cdot \vec{\psi}_r\right)\right) \tag{10}$$

where T_e^+ and T_e^- are the positive and negative torque slopes, respectively. $\tau_s = l_s/R_s$ and $\tau_r = l_r/R_r$.

According to [25], a proper and stable flux regulation is attained when $|\Delta\vec{\psi}_{s.\text{Active}}| > |\Delta\vec{\psi}_{s.Null}|$. Hence, this condition can be written as:

$$|\vec{v}_s \cdot \Delta t_{s1}| > |-\vec{\imath}_s R_s \cdot \Delta t_{s2}| \tag{11}$$

In (11), Δt_{s1} and Δt_{s2} are the time durations in which the active and null voltage vectors are employed to increase and reduce the torque slopes, respectively as shown in Fig. 3. It is worth noting that the condition given by (11) is achieved in the medium and high-speed regions, however, cannot be fulfilled at low speeds owing to the negative torque slope.

The duration of negative torque slope T_e^- gets very large [see Fig. 3(a)] at very low motor speeds under light load torque after touching the reference torque [25]. This causes a long zero-voltage vector to reduce the torque, as depicted by the torque error status (T_{stat}) in Fig. 3(b). Consequently, $\Delta\vec{\psi}_{s.Null}$ becomes

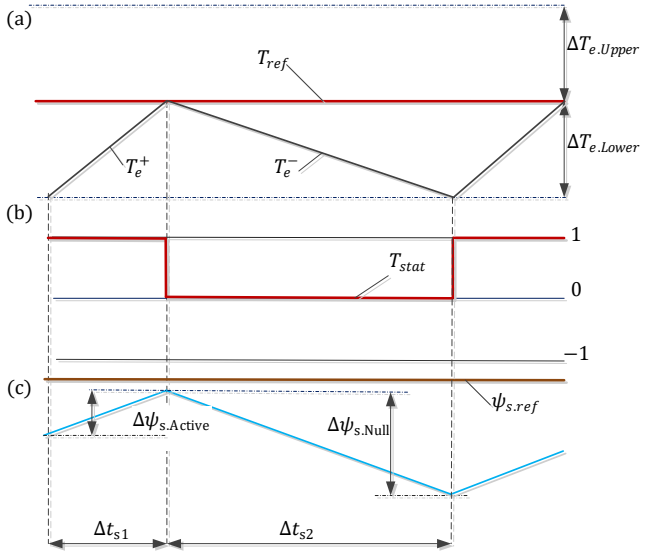

Fig. 3. Waveforms of (a) torque, (b) torque error status, and (c) stator flux.

highly influenced by the stator resistance effect [24], and thus the stator flux magnitude $|\vec{\psi}_s|$ cannot reach its reference value of flux; hence, this causes condition (11) not to be fulfilled, as seen in Fig. 3(c).

C. Impact of Torque Hysteresis Band on Flux Magnitude and Torque at Low Speeds

Since the DTC scheme is implemented in a digital controller, the width of THB and the sampling time must be appropriately designed [27]. It is well-known that the structure of hysteresis-based DTC schemes is very simple, and thus doesn't need large

This article has been accepted for publication in a future issue of this journal, but has not been fully edited. Content may change prior to final publication. Citation information: DOI 10.1109/JESTPE.2019.2897064, IEEE Journal of Emerging and Selected Topics in Power Electronics

computation time. Therefore, the sampling time can be chosen to be small enough to avoid long time duration of torque slopes.

To simplify our discussion in the next section, the nominal and small torque hysteresis bands will be denoted as ΔNT_e (i.e. $\Delta NT_{e.Upper}$ & $\Delta NT_{e.Lower}$) and ΔST_e (i.e. $\Delta ST_{e.Upper}$ & $\Delta ST_{e.Lower}$), respectively. The DTC is typically operated with a nominal THB, ΔNT_e, which is obtained within 10–15% of the rated torque [29] to guarantee that zero-voltage vector is selected, as shown in Fig. 4(a). Nevertheless, if the torque exceeds the upper band of the torque hysteresis owing to the small size of the

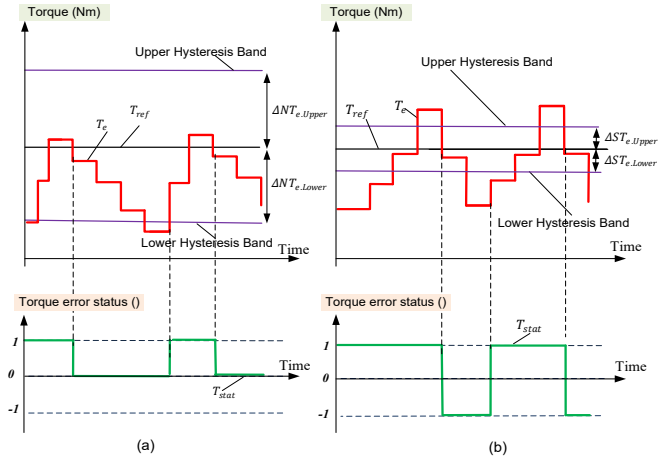

Fig. 4. Comparison of torque and torque error status for (a) nominal THB and (b) small THB.

THB, torque overshoot will occur. As a result, reverse-voltage vectors will be selected, as shown in Fig. 4(b).

According to [25], the selection of reverse-voltage vectors rather than zero-voltage vectors is a suitable solution to fulfill (11) where negative torque slope becomes much steeper with shorter time interval. This is done by using the small THB. It is worth noting that the reverse voltage vectors play a vital role in

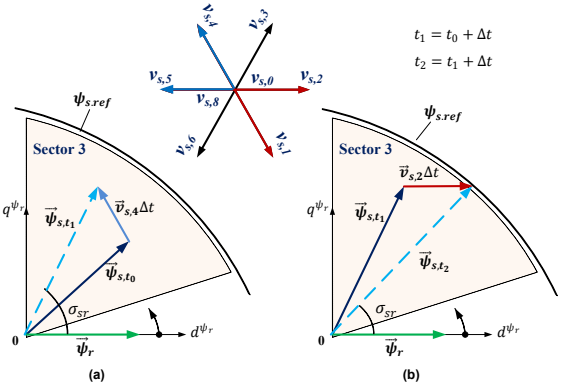

Fig. 5. Behavior of stator flux vector and load angle at low speed of DTC with (a) forward voltage vector followed by (b) reverse voltage vector.

the magnitude of flux and torque ripple. This can be explained and analyzed with the illustration of space vectors of the stator and rotor flux linkages which are moving in the counterclockwise direction at time t_0, t_1 (i.e $t_0 + \Delta t$), and t_2 (i.e. $t_1 + \Delta t$) as shown in Fig. 5. Considering that, the rotor flux moves continuously, while the stator flux moves irregularly with the applied voltage vectors. In this illustration, the stator flux vector $\vec{\psi}_{s,t_0}$ is short and below $\psi_{s.ref}$ within Sector 3, and hence there are four possible voltage vectors in Sector 3; two vectors for the forward direction and two vectors for the reverse direction depending on whether to increase or decrease the stator flux. By considering the small THBs, the voltage vector $\vec{v}_{s,4}$ is initially used (see Fig. 5a) to increase the flux and load angle δ_{sr}. According to (5), the rise in the load angle will lead to the increase of torque. However, the resultant $\vec{\psi}_{s,t_1}$ is still below the reference flux $\psi_{s,ref}$ at t_1 and if zero voltage vector is chosen, this will cause additional shortening of the flux magnitude. In this case, it is desirable to select the reverse

TABLE II
Induction Motor and DTC Parameters

Rated power	3.7 kW	Stator resistance	0.934 ohm
Rated current	8.28 A	Rotor resistance	1.225 ohm
Rated speed	1750 r/min	Stator inductance	146.213 mH
Rated Torque	20.36 Nm	Rotor inductance	146.213 mH
Rated flux	0.6 Wb	Mutual inductance	139.516 mH
Pole pairs		2	

DTC Parameters	
DC Link Voltage, V_{DC}	300 V
Torque hysteresis band (nominal), ΔNT_e	2.5 Nm
Torque hysteresis band (small), ΔST_e	0.01 Nm
Flux hysteresis band, ΔHB_ψ	0.0015 Wb

voltage vector $\vec{v}_{s,2}$ (see Fig. 5b) which will also increase the stator flux $\vec{\psi}_{s,t_2}$ at t_2 and reduces δ_{sr} resulting in a fast reduction of torque according to (5). However, rapid decrease in the torque owing to the reverse voltage vector results in increased torque ripple and higher switching frequency [29].

III. PROPOSED FLUX REGULATION METHOD

The conventional DTC uses a fixed and nominal torque hysteresis band throughout its operation. Therefore, the magnitude of the stator flux becomes significantly affected in a low-speed range, causing the induction machine to be demagnetized. Recently, the work in [28] introduces a simple method that utilizes the alteration of torque hysteresis band to solve this issue. A compromise solution is used to avoid the selection of a small THB at medium and high speeds. In a previous study, the upper and lower bands were simultaneously switched, resulting in continuous active vector switching with no selection of zero-voltage vectors owing to torque overshoot. Although it is capable to regulate the flux, it causes a significant increase in the switching frequency and torque ripple. In order to solve the problems in the previous work, this paper proposes a single THB control that focuses on lessening the negative slope of the torque. Hence, the duration of zero-voltage vectors is reduced, and the number of reverse-voltage vectors is minimized. In this proposed method, the torque overshoot will be reduced by maintaining one of the nominal THBs. An example for the proposed method can be seen in Fig. 6. In the figure, a critical flux point (ψ_c) is used to limit the flux droop region at low motor speeds. The speed ω_r is used in this paper

This article has been accepted for publication in a future issue of this journal, but has not been fully edited. Content may change prior to final publication. Citation information: DOI 10.1109/JESTPE.2019.2897064, IEEE Journal of Emerging and Selected Topics in Power Electronics

for its easy implementation, as shown in Fig. 7. The critical

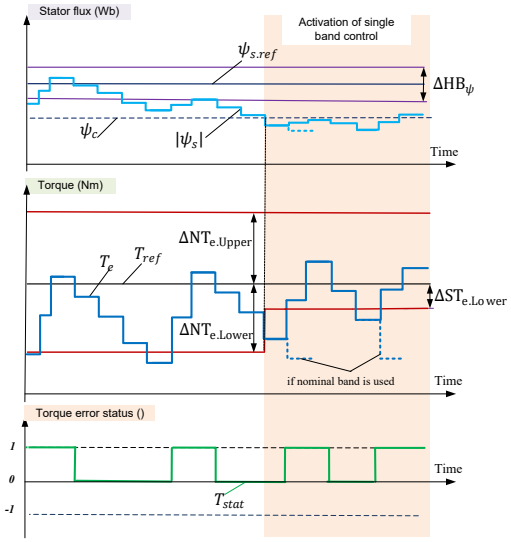

Fig. 6 Schematic of stator flux, torque, and torque status by using single THB control in forward direction.

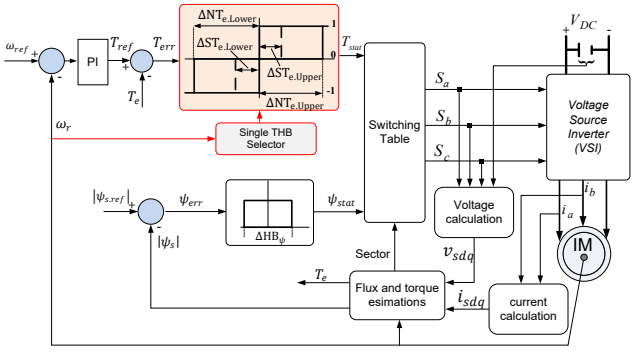

Fig. 7. Diagram of DTC-hysteresis-based IM with the proposed control strategy.

speed with respect to the critical flux point can be denoted as $\omega_r^{\psi c}$. As such, the proposed dynamic THB of the DTC will operate in the forward direction based on (12) and in the reverse direction based on (13).

$$HTB = \begin{cases} \Delta NT_{e.Upper} \ \& \ \Delta NT_{e.Lower}, & \omega_r > \omega_r^{\psi c} \\ \Delta NT_{e.Upper} \ \& \ \Delta ST_{e.Lower}, & 0 \le \omega_r \le \omega_r^{\psi c} \end{cases} \quad (12)$$

$$HTB = \begin{cases} \Delta ST_{e.Upper} \ \& \ \Delta NT_{e.Lower}, & -\omega_r^{\psi c} \le \omega_r < 0 \\ \Delta NT_{e.Upper} \ \& \ \Delta NT_{e.Lower}, & \omega_r < -\omega_r^{\psi c} \end{cases} \quad (13)$$

IV. SIMULATION RESULTS

Simulation of a DTC-hysteresis-based induction machine is developed in the PSIM software platform to validate the effectiveness of the proposed flux regulation method. The system parameters and DTC values are listed in Table II.

The nominal THB is selected at 2.5 Nm, which is within 10 to 15% of the rated torque. The small THB is set at 0.01 Nm (0.5% of rated torque), which is not an optimum threshold value for a small THB. However, this value is chosen to ensure that the duration of negative torque slope does not become very

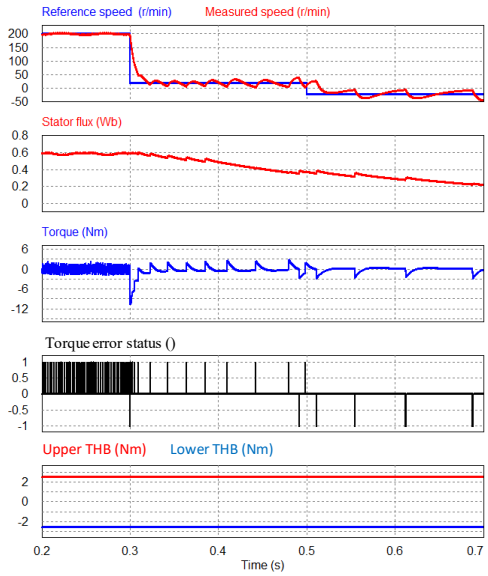

Fig. 8 Simulation results for the original DTC of IM under light load.

large, and hence, increasing the time interval of zero voltage vectors.

For ease of comparison, the conventional DTC schemes with controlled bands are referred to as follows:

1) DTC-HB1: DTC with controlled THB using both upper

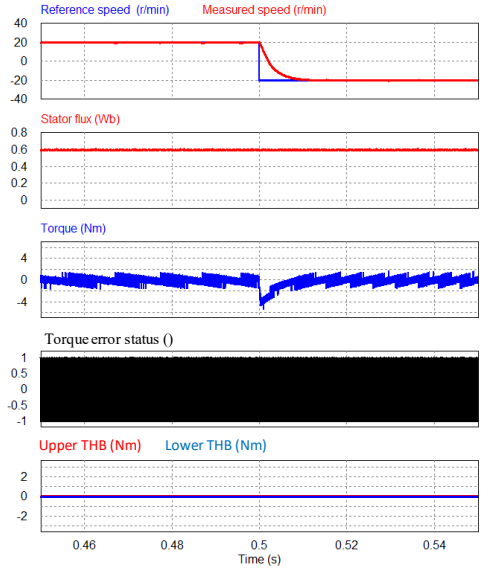

Fig. 9 Simulation results at 20 and -20 r/min for DTC-HB1 of IM under light load.

and lower THBs [24].

2) DTC-HB2: Proposed DTC with controlled THB using either upper or lower THBs according to (12) and (13).

The sampling time of the classical DTC, DTC-HB1 and DTC-HB1 schemes is 50 μs. It is worth noting that in both simulation and experiments, the critical flux droop was found

This article has been accepted for publication in a future issue of this journal, but has not been fully edited. Content may change prior to final publication. Citation information: DOI 10.1109/JESTPE.2019.2897064, IEEE Journal of Emerging and Selected Topics in Power Electronics

empirically for the system tested in this paper. Therefore, the critical speed $\omega_r^{\psi c}$ is 70 r/min.

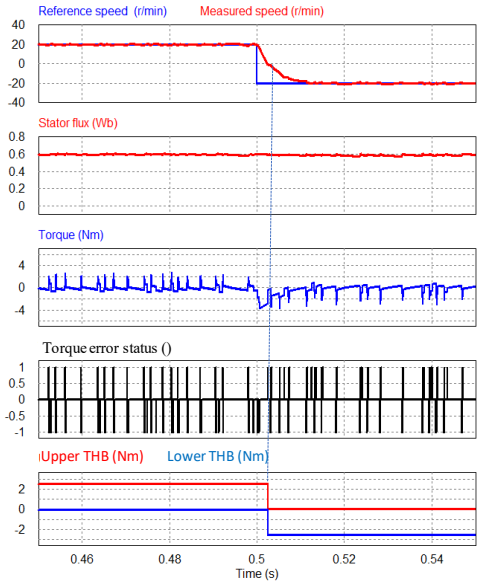

Fig. 10 Simulation results at 20 and -20 r/min for DTC-HB2 of IM under light load

Figs. 8, 9, 10 depict the results of speed, stator flux, torque, torque error status, and upper and lower torque hysteresis bands under light load for the classical DTC, DTC-HB1 and DTC-HB2, respectively. It is noteworthy that light load is the worst-case condition for flux droop because the duration of negative torque slopes gets larger [27]. Fig. 8 shows the response of the classical DTC with nominal THBs at 200 rpm, 20 rpm, and -20 rpm. It can be observed that at 200 rpm the stator flux is well established; however, when the speed reference steps down to 20 r/min, which is below the speed critical region, the flux droop begins, and hence causing serious oscillations on the speed waveform. The stator flux continues to drop and becomes even worse when the speed reverses to - 20 r/min. It can be noted that the duration of zero voltage vectors keeps incrementing owing to the increase in the time duration of negative torque slope.

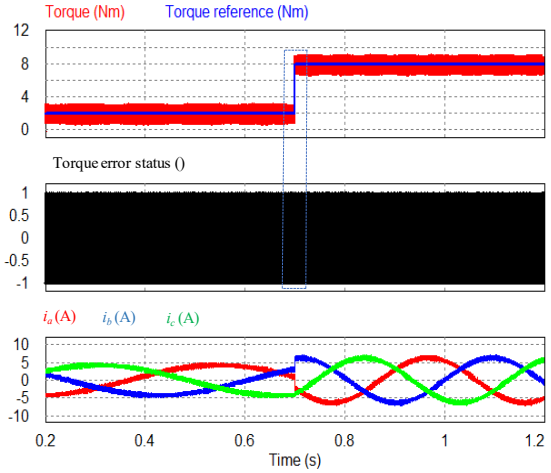

Fig. 11 Simulation result of the torque step response from 2 to 8 Nm at 60 r/min for DTC-HB1 of IM.

Figs.9 and 10 illustrate the performance for DTC-HB1 and DTC-HB2 below the critical speed region in forward (20 r/min) and reverse (-20 r/min) motor directions. When reducing both torque hysteresis bands in DTC-HB1, excessive switching of torque error statuses is generated. This leads to large torque ripples and very high switching of voltage as indicated by the

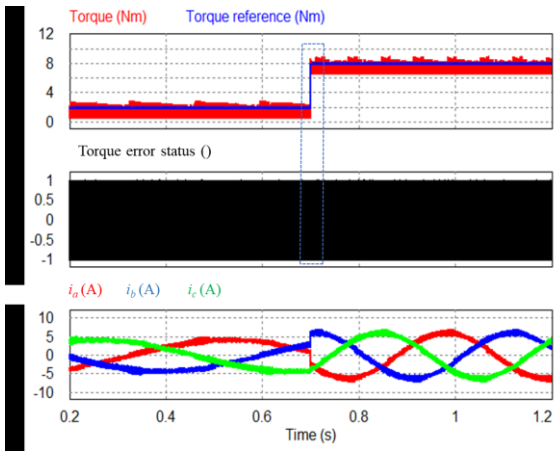

Fig. 12 Simulation result of the torque step response from 2 to 8 Nm at 60 r/min for DTC-HB2 of IM.

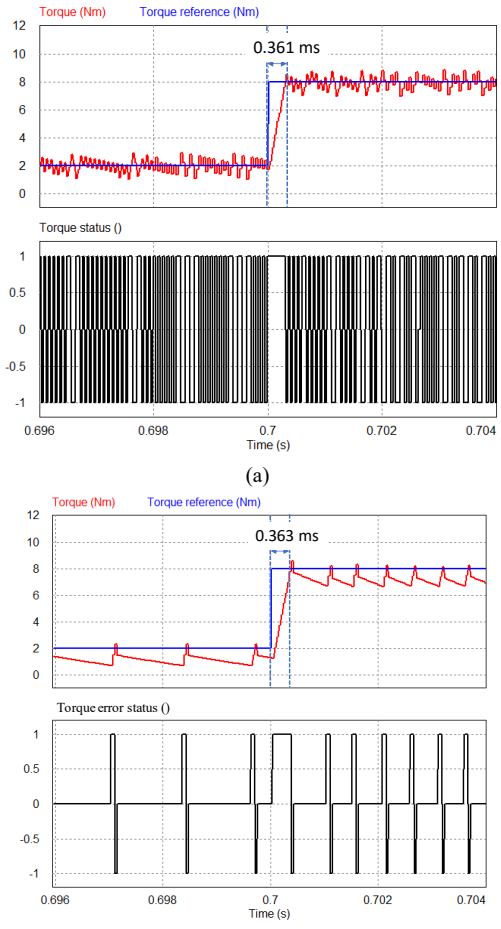

Fig. 13 Zoomed simulation results of the torque step response from 2 to 8 Nm for (a) DTC-HB1 and (b) DTC-HB2 of IM.

This article has been accepted for publication in a future issue of this journal, but has not been fully edited. Content may change prior to final publication. Citation information: DOI 10.1109/JESTPE.2019.2897064, IEEE Journal of Emerging and Selected Topics in Power Electronics

torque error status as shown in Fig. 9. By contrast, in the proposed DTC-HB2 method one of the THBs is switched

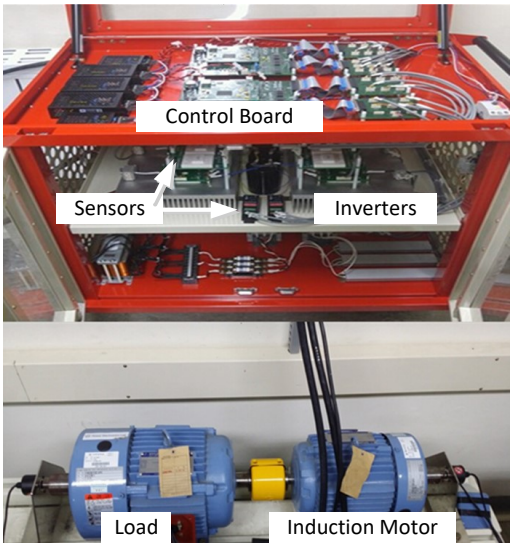

Fig. 14 Experimental setup.

depending on the motor direction according to (12) and (13). It can be seen that when the speed is in the forward direction, the $\Delta NT_{e.Upper}$ and $\Delta ST_{e.Lower}$ are selected as show in Fig. 10. However, when the speed reference became less than 0 r/min, the positions of THBs automatically switched with respect to (13). As a result, the proposed DTC-HB2 can still regulate the stator flux, and in addition, reduce the torque ripple, as seen in Fig. 10. This agrees with our analysis, which focuses on

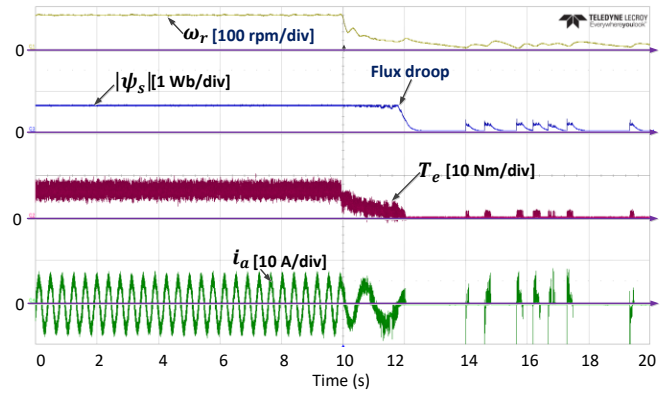

Fig. 15 Experimental results of the classical DTC with nominal THBs.

minimizing the duration of the zero-voltage vectors and thus decreasing the switching frequency of the reverse-voltage vectors. Hence, the proposed method exhibits higher efficiency by inspecting the reduction in the switching signals indicated by the torque error status while maintaining the flux regulation.

Figs. 11 and 12 show the dynamic responses for DTC-HB1 and DTC-HB2 at a speed load of 60 r/min when the reference torque changes from 2 to 8 Nm. The waveforms (from top to bottom) are the torque, torque error status, and stator phase currents (i_{as}, i_{bs}, i_{cs}). The phase currents in both methods show good sinusoidal waveforms. However, it is clear that the torque ripple in the proposed DTC-HB2 is reduced when compared to that of DTC-HB1. The areas within the dashed rectangular in both Figs. 11 and 12 are zoomed in Fig. 13 for better comparison between the two methods. It can be observed that both DTC-HB1 and DTC-HB2 control algorithms exhibit fast dynamic response as the torque response times of DTC-HB1 and DTC-HB2 approaches are very close with 0.361 ms versus 0.363 ms, respectively. Once again, it is seen that DTC-HB1 exhibits very high switching of active voltage vectors as indicated by the torque error status as shown in Fig. 13 a. In contrast, the proposed DTC-HB2 exhibits less switching by including the zero voltage vectors as seen in Fig.13 b. However, when the torque reference changes to 8 Nm in the proposed DTC-HB2 approach, this results in shorter time duration of negative torque slope. In fact, higher level of torque reference causes shorter zero voltage vectors and, hence, higher torque switching when compared to low level of torque reference as discussed in [27].

V. IMPLEMENTATION AND EXPERIMENTAL VERIFICATION

To investigate the feasibility of the proposed flux regulation strategy on DTC-hysteresis-based induction machine, the experimental setup shown in Fig. 14 is realized. It consists of a DSP 28335 control board and a three-phase intelligent power module equipped with IGBTs. A 2000 PPR encoder was used to obtain the measured speed. To load the machine, a 5.5-kW IM controlled by a commercial Yasukawa inverter was used.

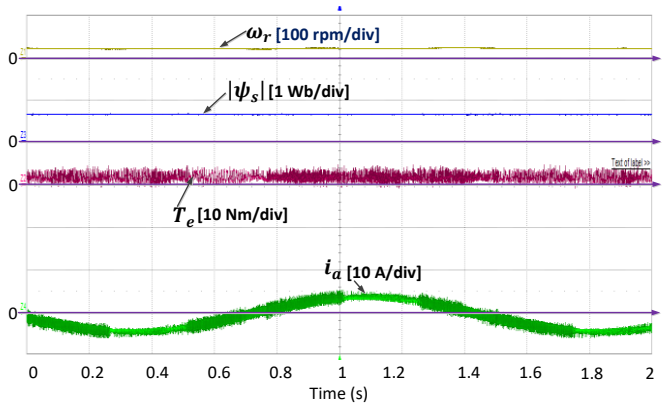

Fig. 16 Experimental results of DTC-HB1 at 20 r/min under light load.

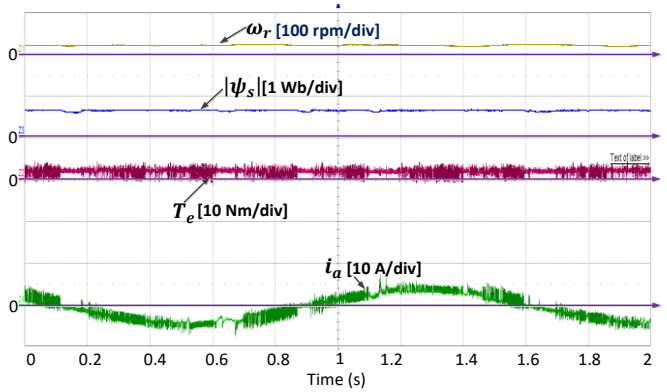

Fig. 17 Experimental results of proposed DTC-HB2 at 20 r/min under light load.

This article has been accepted for publication in a future issue of this journal, but has not been fully edited. Content may change prior to final publication. Citation information: DOI 10.1109/JESTPE.2019.2897064, IEEE Journal of Emerging and Selected Topics in Power Electronics

The sampling time of the DTC algorithms, including the proposed method is 50 µs. The parameters of the IM motor are listed in Table II, which are similar to the simulation.

Before applying the proposed method, first, the performance of a conventional DTC with nominal THB is illustrated in Fig. 15 when the speed steps below the critical speed region (i.e., from 80 to 20 r/min). Simultaneously, the applied load torque decreases from 6 to 2 Nm. It is clearly seen that the performance of the stator flux starts to deteriorate at very low speeds, especially when the load torque becomes light. As a result, the corresponding waveforms of the speed, torque, and current become significantly distorted and aggravated

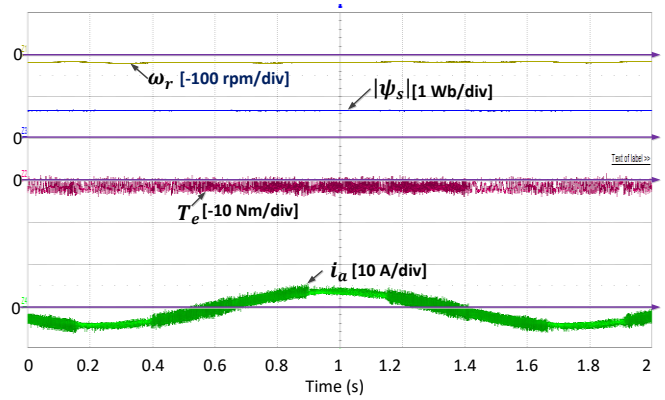

Fig. 18 Experimental results of DTC-HB1 at -20 r/min under light load.

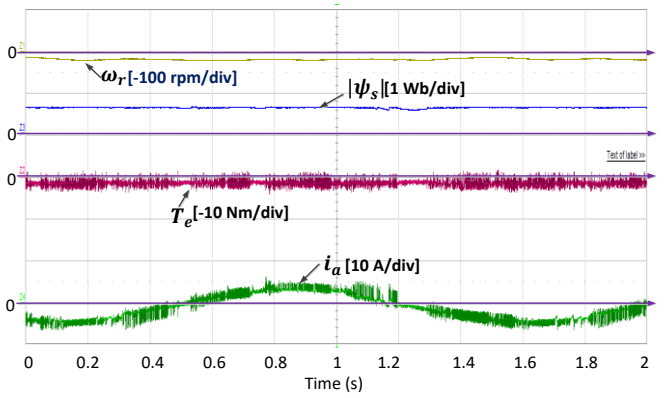

Fig. 19 Experimental results of proposed DTC-HB2 at -20 r/min under light load.

A. *Steady-State Operation*

In this subsection, the experimental results of the steady-state responses for the DTC-HB1 and proposed DTC-HB2 methods are presented. It is worth noting that the experiments are carried out below the critical speed region. Figs. 16–19 show (from top to bottom) the rotor speed, stator flux, electrical torque, and stator current when the IM operates at 20 and -20 r/min with a light load torque of 2 Nm. Figs. 16 and 18 show the experimental results of DTC-HB1; as in the simulation, both THBs are switched to ΔST_e. It can be observed that DTC-HB1 can provide a well-regulated stator flux in both motor directions owing to very high switching of the active voltage vectors.

Nevertheless, this results in higher torque and current ripples and decreases the efficiency of the system, as indicated by the waveforms of the torque error status in Fig. 9. Conversely, the proposed method DTC-HB2 shows almost comparable results in terms of flux regulation and rotor speed for both motor directions, as shown in Fig. 17 and 19. In addition, the proposed method can contribute to less torque and current ripple in both motor directions, as shown in Fig. 17 and 19. More importantly, the proposed DTC strategy contributes to a reduction of the switching frequency by incorporating the zero-voltage vectors as discussed in the simulation (see Fig. 10).

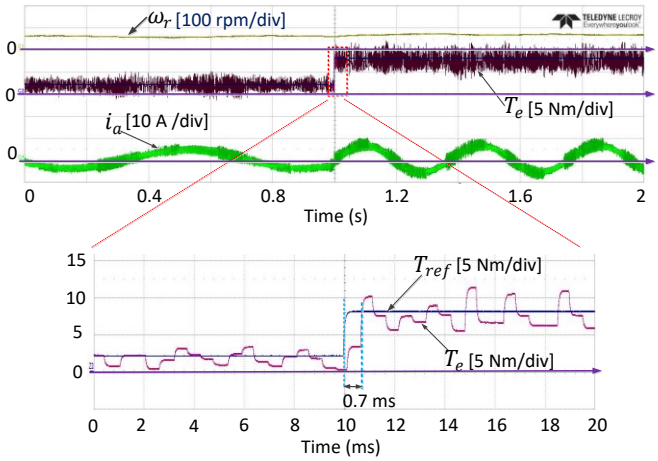

Fig. 20 Experimental results at 60 r/min with torque step response from 2 to 8 Nm for DTC-HB1.

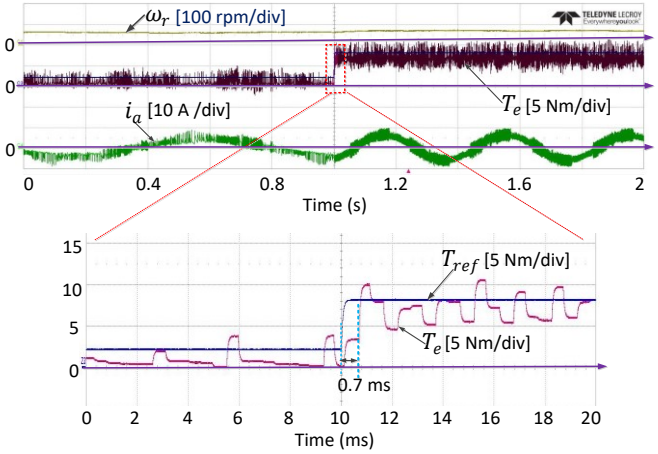

Fig. 21 Experimental results at 60 r/min with torque step response from 2 to 8 Nm for the proposed DTC-HB2.

B. *Transient-State Operation*

Figs. 20 and 21 show the dynamic torque responses for the DTC-HB1 and proposed DTC-HB2, respectively. The load is at 60 r/min (i.e., below the critical speed region) with a torque change from 2 to 8 Nm. It is apparent that the performance of the proposed DTC-HB2 is smaller than that of the conventional DTC-HB1 in terms of the torque ripples. Nevertheless, it can be observed that DTC-HB1 and DTC-HB2 have a comparable dynamic response time with 0.7ms because both methods require only active forward voltage vectors during transient state (see Fig. 13). It is worth noting that there is a bandwidth limitation in the data acquisition system. This is why the torque response times for simulation and experimental results are not the same. Nevertheless, both methods can still maintain the

quick dynamic torque performance of the original DTC. It is due to the fact that the selection of forward-voltage vectors during the transient state can enlarge the load angle in (5), thus increasing the torque response, as previously explained. Furthermore, the speed and current waveforms show good robustness and stability against the disturbance in both DTC strategies.

VI. CONCLUSION

In this paper, a simple flux regulation strategy during low-speed operation is proposed for the direct torque control of an induction motor. Narrowing the upper and lower widths of the torque hysteresis bands from nominal to small values at low speeds will obtain flux regulation at the cost of very high switching of active voltage vectors owing to the torque overshoot. As a result, the torque and current ripples will increase. Conversely, the proposed method controls only a single torque hysteresis band strategy to reduce the period of the zero-voltage vectors. This minimizes the torque ripple and flux regulation. The main benefit of the proposed method is its simplicity and ability to improve the efficiency of the system. Simulation and experimental results were presented to verify the effectiveness of the proposed single-THB control strategy.

REFERENCES

[1] I. Takahashi and T. Noguchi, “A new quick-response and high efficiency control strategy of an induction motor,” *IEEE Trans. Ind. Appl*., vol. IA-22, no. 5, pp. 820-827, Sep. 1986.

[2] M. Depenbrock, “Direct self control for high dynamics performance of inverter feed AC machines,”*ETZArch.,* vol. 7, no. 7, pp. 211–218, 1985.

[3] ‘Direct Torque Control Comes to AC Drives’, *Control Engineering*, March 1995, vol. 42, no. 3, p. 9.

[4] K. B. Lee and F. Blaabjerg, "A Modified DTC-SVM for Sensorless Matrix Converter Drives Using a Simple Deadbeat Control," *HAIT Journal of Science and Engineering B*, vol. 2, no. 5-6, pp. 715-735, 2005.

[5] C. Lascu, I. Boldea, and F. Blaabjerg, "A modified direct torque control for induction motor sensorless drive," *IEEE Trans. Ind. Appl.,* vol. 36, pp. 122-130, 2000.

[6] Y.-S. Lai and J.-H. Chen, “A new approach to direct torque control of induction motor drives for constant inverter switching frequency and torque ripple reduction,” *IEEE Trans. Energy Convers.*, vol. 16, no. 3, pp. 220–227, Sep. 2001.

[7] J. Rodriguez et al., "State of the Art of Finite Control Set Model Predictive Control in Power Electronics," *IEEE Trans. Ind. Informat.,* vol. 9, no. 2, pp. 1003-1016, 2013.

[8] W. Fengxiang, Z. Zhenbin, S. Alireza Davari, R. Fotouhi, D. Arab Khaburi, J. Rodriguez, et al., "An Encoderless Predictive Torque Control for an Induction Machine With a Revised Prediction Model and EFOSMO," *IEEE Trans. Ind. Electron.*, vol. 61, pp. 6635-6644, 2014.

[9] M. H. Vafaie, B. M. Dehkordi, P. Moallem, and A. Kiyoumarsi, "Minimizing Torque and Flux Ripples and Improving Dynamic Response of PMSM Using a Voltage Vector With Optimal Parameters," *IEEE Trans. Ind. Electron.*, vol. 63, no. 6, pp. 3876–3888, 2016..

[10] Y. Cho, Y. Bak, and K. B. Lee, "Torque-Ripple Reduction and Fast Torque Response Strategy for Predictive Torque Control of Induction Motors," *IEEE Trans. Power Electron*., vol. PP, no. 99, pp. 1-1, 2017.

[11] M. E. Zarei, C. Veganzones Nicolás and J. Rodríguez Arribas, "Improved Predictive Direct Power Control of Doubly Fed Induction Generator During Unbalanced Grid Voltage Based on Four Vectors," *IEEE J. Emerg. Sel. Topics Power Electron.*, vol. 5, no. 2, pp. 695-707, June 2017.

[12] T. Geyer, G. Papafotiou, and M. Morari, "Model Predictive Direct Torque Control—Part I: Concept, Algorithm, and Analysis," *IEEE Trans. Ind. Electron.*, vol. 56, no. 6, pp. 1894-1905, 2009.

[13] P. Tiitinen and M. Surandra, "The next generation motor control method, DTC direct torque control," *in Proc. Int. Conf. Power Eelectronics, Drives and Energy System for Industrial Growth*, 1996, pp. 37-43.

[14] J. N. Nash, "Direct torque control, induction motor vector control without an encoder," *IEEE Trans. Ind. Appl*., vol. 33, no. 2, pp. 333-341, March-April 1997.

[15] G. S. Buja and M. P. Kazmierkowski, "Direct torque control of PWM inverter-fed AC motors - a survey," *IEEE Trans. Ind. Electron*., vol. 51, no. 4, pp. 744-757, 2004.

[16] C. Patel, R. P. P. A. Day, A. Dey, R. Ramchand, K. Gopakumar, and M. P. Kazmierkowski, "Fast Direct Torque Control of an Open-End Induction Motor Drive Using 12-Sided Polygonal Voltage Space Vectors," *IEEE Trans. Power Electron.*, vol. 27, no. 1, pp. 400-410, 2012.

[17] K. B. Lee, J. H. Song, I. Choy and J. Y. Yoo, "Improvement of low-speed operation performance of DTC for three-level inverter-fed induction motors," *IEEE Trans. Ind. Electron*., vol. 48, no. 5, pp. 1006-1014, 2001.

[18] S. S. Sebtahmadi, H. Pirasteh, S. H. A. Kaboli, A. Radan, and S. Mekhilef, "A 12-Sector Space Vector Switching Scheme for Performance Improvement of Matrix-Converter-Based DTC of IM Drive," *IEEE Trans. Power Electron.*, vol. 30, no. 7, pp. 3804-3817, 2015.

[19] D. Mohan, X. Zhang and G. H. B. Foo, "Three-Level Inverter-Fed Direct Torque Control of IPMSM With Torque and Capacitor Voltage Ripple Reduction," *IEEE Trans. Energy Convers*., vol. 31, no. 4, pp. 1559-1569, Dec. 2016.

[20] K. B. Lee, J. H. Song, I. Choy and J. Y. Yoo, "Improvement of low-speed operation performance of DTC for three-level inverter-fed induction motors," *IEEE Trans. Ind. Electron*., vol. 48, no. 5, pp. 1006-1014, 2001.

[21] S. S. Sebtahmadi, H. Pirasteh, S. H. A. Kaboli, A. Radan, and S. Mekhilef, "A 12-Sector Space Vector Switching Scheme for Performance Improvement of Matrix-Converter-Based DTC of IM Drive," *IEEE Trans. Power Electron*., vol. 30, no. 7, pp. 3804-3817, 2015.

[22] D. Mohan, X. Zhang and G. H. B. Foo, "Three-Level Inverter-Fed Direct Torque Control of IPMSM With Torque and Capacitor Voltage Ripple Reduction," *IEEE Trans. Energy Convers.,* vol. 31, no. 4, pp. 1559-1569, Dec. 2016.

[23] M. P. Kazmierkowski and A. Kasprowicz, "Improved direct torque and flux vector control of PWM inverter-fed induction motor drives," *IEEE Trans. Ind. Electron.*, vol. 42, pp. 344–350, Aug. 1995.

[24] T. Noguchi, M. Yamamoto, S. Kondo, and I. Takahashi, "High frequency switching operation of PWM inverter for direct torque control of induction motor," *in Conf. Rec. IEEE-IAS Annu. Meeting*, 1997, pp. 775–780.

[25] I. M. Alsofyani and N. R. N. Idris, "Simple Flux Regulation for Improving State Estimation at Very Low and Zero Speed of a Speed Sensorless Direct Torque Control of an Induction Motor," *IEEE Trans. Power Electron*., vol. 31, pp. 3027-3035, 2016.

[26] W.S.H. Wong and D. Holliday, “Minimisation of flux droop in direct torque controlled induction motor drives,” *in Proc. IEEE Electric Power ppl*., vol. 151, no. 6, pp. 694–703, Nov. 7, 2004.

[27] I. M. Alsofyani, N. R. N. Idris and K. Lee, "Dynamic Hysteresis Torque Band for Improving the Performance of Lookup-Table-Based DTC of Induction Machines," *IEEE Trans. Power Electron.*, vol. 33, no. 9, pp. 7959-7970, Sept. 2018.

[28] I. M. Alsofyani, N. R. N. Idris, and Y. A. Alamri, "An improved flux regulation using a controlled hysteresis toque band for DTC of induction machines," *in Proc. IEEE Conf. Energy Convers*., 2015, pp. 368-372.

[29] N. R. N. Idris and A. H. M. Yatim, "Direct torque control of induction machines with constant switching frequency and reduced torque ripple," *IEEE Trans. Ind. Electron*., vol. 51, pp. 758-767, 2004.

[30] N. R. N. Idris and A. H. M. Yatim, "Direct torque control of induction machines with constant switching frequency and reduced torque ripple," *IEEE Trans. Ind. Electron*., vol. 51, pp. 758-767, 2004.

Ibrahim Mohd Alsofyani (M'16) received M.Eng. degree in electrical mechatronics and automatic control and the Ph.D. degree both from the Universiti Teknologi Malaysia, Johor Bahru, Malaysia, in 2011 and 2014, respectively. From 2014 to 2016, he was a research associate and then postdoctoral fellow at the UTM-PROTON Future Drive Laboratory, Universiti Teknologi Malaysia. From 2016 to 2017, he worked as a lecturer in the Faculty of Engineering, Lincoln University College, Selangor, Malaysia. In 2017 , he was a research professor and then became an assistant professor in 2018 at the School of Electrical and Computer Engineering, Ajou University, Suwon, Korea. His current research interests include electric machine drives, renewable power generations and electric vehicle applications.

Dr. Alsofyani was the recipient of the Brain Korea 21 (BK21) Program Scholarship in 2017.

Keon Young Kim (S'17) received the B.S. and M.S. degrees in electrical and computer engineering from Ajou University, Suwon, South Korea, in 2017 and 2019, respectively.

Since 2019, he has been with the Advanced Drive Technology, Anyang, South Korea. His research interests include electric machine drives, matrix converter, and grid-connected systems.

.

Sze Sing Lee (S'11–M'14–SM'18) received the B.Eng. (Hons.) and Ph.D. degrees in electrical engineering from the Universiti Sains Malaysia, Malaysia, in 2010 and 2013, respectively.

He is currently an Assistant Professor with the University of Southampton, Malaysia and a Visiting Scholar with Ajou University, South Korea. His research interests include power converter/inverter topologies and their control strategies.

Dr. Lee received the International Scholar Exchange Fellowship from Korea Foundation for Advanced Studies.

.

Kyo-Beum Lee (S'02–M'04–SM'10) received the B.S. and M.S. degrees in electrical and electronic engineering from the Ajou University, Suwon, Korea, in 1997 and 1999, respectively. He received the Ph.D. degree in electrical engineering from the Korea University, Seoul, Korea, in 2003. From 2003 to 2006, he was with the Institute of Energy Technology, Aalborg University, Aalborg, Denmark. From 2006 to 2007, he was with the Division of Electronics and Information Engineering, Chonbuk National University, Jeonju, Korea.

In 2007, he joined the School of Electrical and Computer Engineering, Ajou University, Suwon, Korea. He is an associated editor of the IEEE Transactions on Power Electronics, the Journal of Power Electronics, and the Journal of Electrical Engineering & Technology. His research interests include electric machine drives, renewable power generations, and electric vehicle applications.

.